Eur J Forest Res (2013) 132:151–163
DOI 10.1007/s10342-012-0664-z

ORIGINAL PAPER

Greater abundance of *Fagus sylvatica* in coniferous flood protection forests due to climate change: impact of modified root densities on infiltration

Benjamin Lange · Peter F. Germann · Peter Lüscher

Received: 9 March 2012 / Revised: 21 August 2012 / Accepted: 2 October 2012 / Published online: 4 November 2012

Abstract Climate change is expected to modify the spatial distributions of zonal forest communities and thus, their species compositions. The aim of this paper was to study the impact of higher abundance of beech on water storage capacity in current coniferous flood protection forests due to varying root densities of the main tree species. Two forest communities in the northern pre-Alps in Switzerland with similar soil properties but varying in species composition were investigated (space-for-time substitution). It was assumed that the Vaccinio myrtillii-Abieti-Piceetum (site A) will be replaced by a Luzulo-Abieti-Fagetum (site B). We irrigated 16 hydromorphic soils (1 m^2, 70 mm/h, three consecutive irrigations) at site A and 10 at site B and recorded water-content variations with time domain—and frequency domain reflectometry. Roots were extracted from soil cores taken from the positions where the water-content probes were inserted, and digitally measured. Infiltration capacity ω_I was mainly limited to the upper soil at site A but was approximately constant down to 0.7 m depth at site B. Between 0.3 and 1.0 m soil depth, root densities at site B exceeded those at site A. Root density was the main predictor for ω_I ($R^2 = 0.57$) at site A as shown by a multiple linear regression analysis. Assuming that the root density in the current coniferous forest (A) will increase to that of the beech stand (B) due to the greater abundance of beech, the water storage capacity will increase by 9.2 mm in consequence of the expected forest transformation.

Keywords Climate change · Flood protection forests · Water storage capacity · Beech · Spruce · Forest transformation

Communicated by C. Ammer.

B. Lange · P. Lüscher
Swiss Federal Institute for Forest, Snow and Landscape Research WSL, Zürcherstrasse 111, 8903 Birmensdorf, Switzerland

B. Lange (✉)
In der Wässeri 37, 8047 Zürich, Switzerland
e-mail: b.lange@gmx.ch

P. F. Germann
Department of Geography, University of Bern, Hallerstrasse 12, 3012 Bern, Switzerland

Introduction

Climate change is expected to increase the annual mean temperature in the northern part of Switzerland by approximately 2 °C by 2050 compared with 1990 (OcCC/ProClim-(ed.) 2007). As a consequence, the spatial distribution of zonal forest communities and thus the species compositions of these forests will be modified by temperature increase.

Approximately 36 % of the total forested area in Switzerland has an important protection function (Brändli 2010). Flood protection forests are likely to become even more necessary since floods are expected to occur more frequently due to climate change (OcCC/ProClim-(ed.) 2007). Such forests are in the catchment areas of the large Swiss rivers and are located in the montane and subalpine belts. Simulations indicate that the currently dominant Piceo-Abietion community in the northern pre-Alps in Switzerland will be replaced by Abieti-Fagion (Brzeziecki et al. 1995). Thus, the abundance of *Fagus sylvatica* will increase at the expense of *Picea abies* and, to a lesser extent, of *Abies alba*. This forest transformation may influence the efficiency of these flood protection forests.

Species change in forests impacts their hydrological properties directly by modifying their transpiration and

interception rates. The interception rates of deciduous trees vary during the course of the year, while those of evergreen conifers remain nearly constant throughout all seasons (Christiansen et al. 2006). Furthermore, the transpiration rates of conifers and deciduous trees differ. Peck and Mayer (1996) analysed several studies about transpiration rates of trees and concluded that beech transpires on average 27 % more than Norway spruce, even though the transpiration of beech is mainly limited to the growing season. Hence, tree species significantly influence the soil water content and, consequently, how much water the soil can potentially store.

The transformation of forest composition also affects soil hydrological characteristics indirectly by modifying soil properties. The thickness of the forest floor layer declined during a *Pinus sylvestris* to *F. sylvatica* transformation in Germany, but the humus topsoil increased (Bens et al. 2007). Organic layers have high water storage capacities (Guevara-Escobar et al. 2007), but may also reduce infiltration capacity as they are water repellent (e.g. Doerr et al. 2000). Moreover, changes in tree species impact the rhizosphere since different species have different root systems and root densities, resulting in varying spatial patterns of water uptake, and thus drying out of the soils (Schwärzel et al. 2009).

Roots are important generators of preferential flow paths, which may improve the forest soil's infiltration capacity substantially (Beven and Germann 1982). Noguchi et al. (1999) demonstrated that 70 % of the macropores in the topsoil and 55 % in the subsoil in a Japanese forest were related to roots. Lange et al. (2009, 2010) compared the root distributions in hydromorphic soils with the porosity that effectively carried preferential flow, and concluded that root density was related to infiltration capacity. Pores generated by woody roots can persist for decades, as has been shown in Denmark and Switzerland (Jorgensen et al. 2002; Hagedorn and Bundt 2002). Furthermore, saturated hydraulic conductivity k_s can be improved by roots since Li and Ghodrati (1994) found that k_s was five to six times higher in samples with root channels than in those without roots. Thus, roots seem to be one of the most important generators of well-connected pores in forest soils. Periodical anaerobic conditions in soils limit the root growth of certain species. Lehnardt and Brechtel (1980) found the roots of adult beech stands penetrated down to 0.6 m, whereas the maximum root depth of spruce was only 0.4 m in comparable hydromorphic soils, indicating that spruce is more liable to oxygen deficiency in the rhizosphere.

Pores generated by roots are of particular importance for infiltration in forest stands growing on poorly drainable forest soils (Lüscher and Zürcher 2003; Lange et al. 2009). A species shift in such stands may influence the soil's infiltration capacity and, hence, the flood protective function. Even though it is widely accepted that roots are important for infiltration and that climate change will result in a forest transformation, the significance of these processes for flood protection has, as far as we know, never been explored. Thus, the main objective of this study was to investigate how an increasing abundance of beech in coniferous flood protection forest stands on hydromorphic soils in Switzerland will affect infiltration and water retention due to the resulting modified root densities and distributions. In particular, we aimed to:

(i) compare the infiltration characteristics of two forest sites with comparable soil properties but varying abundances of beech and spruce;
(ii) evaluate the relevance of roots and other soil properties for infiltration characteristics and
(iii) model the modification of water storage capacity resulting from the greater abundance of beech in coniferous flood protection forests.

Materials and methods

Site and soil description

The experiments were conducted in the Gantrisch region in the Swiss pre-Alps approximately 30 km south of Berne at altitudes between 880 and 1,000 m a.s.l. Annual precipitation averages 1,700 mm and the mean annual temperature is 5.9 °C at 1,160 m a.s.l. (Zimmermann et al. 2006). The study sites are located in the Flysch zone and features mainly marled clays interlaced with stony or sandy layers. A space-for-time substitution was applied to evaluate the potential effects of greater abundance of beech in the flood protection forest, currently composed of spruce and fir. Two adult forest sites with comparable soil properties but varying in forest composition and altitude were investigated. The distance between the sites is approximately 700 m and the difference in the altitude $\approx$120 m. Site A defines the current forest stand and is classified as a Vaccinio myrtillii-Abieti-Piceetum (Ellenberg and Klötzli 1972), with Norway spruce (*P. abies* (L.) Karst.) as the most abundant species. Silver fir (*A. alba* Miller) and European beech (*F. sylvatica* L.) are secondary.

The prevailing soil types are Gleys, cambic Gleys, gleyic and stagnic Cambisols and Cambisols, according to FAO-UNESCO (1988). Beneath depths of 0.03–0.25 m, hydromorphic attributes such as iron and manganese concretions and mottles are found. The physical and chemical properties of the soil were determined from dried samples (48 h, 105 °C for bulk density and 60 °C for pH and texture). Three cylinders per horizon, with a volume of

1,000 cm^3 and a height of 0.1 m, were collected to determine bulk density. pH was determined in a $CaCl_2$ solution and the pipette method was applied for particle-size distribution separation. Considering all horizons investigated at site A, the percentage of sand was 18.6–71.6 %, silt content was 12.7–43.5 % and clay varied between 9.9 and 42.0 %. Bulk density was between 0.19 and 1.19 Mg m^{-3} in topsoils and 0.75 and 1.60 Mg m^{-3} in subsoils. The slopes of the investigated areas did not exceed 15°.

Climate change will enhance the abundance of beech in what are currently mainly coniferous forests in the montane belt (Brzeziecki et al. 1995). Thus, the second area investigated (site B) was a Luzulo-Abieti-Fagetum (Ellenberg and Klötzli 1972), which is what will presumably replace the current Vaccinio myrtillii-Abieti-Piceetum with global warming. This stand is characterised by more abundant European beech, while silver fir and especially Norway spruce are less dominant. Figure 1 shows a map of the investigated areas. The prevailing soil types are Gleys according to FAO-UNESCO (1988), and hydromorphic attributes are found beneath depths of 0.05–0.14 m. Soil texture varied between 17.5 and 73.1 % sand, 16.4 and 48.6 % silt and 8.6 and 34.6 % clay. Bulk density was 0.65–1.00 Mg m^{-3} in topsoils and 0.79–1.60 Mg m^{-3} in subsoils. The slopes of the areas investigated were less than 7°.

Table 1 summarises the characteristics of the study sites and Fig. 2 compares generalised soil profiles and average thicknesses of classes of soil genetic horizons. Both sites are characterised by an organic layer of 0.04–0.05 m above non-hydromorphic horizons with average thicknesses between 0.12 and 0.13 m, following by a layer with only few hydromorphic features up to approximately 0.3 m.

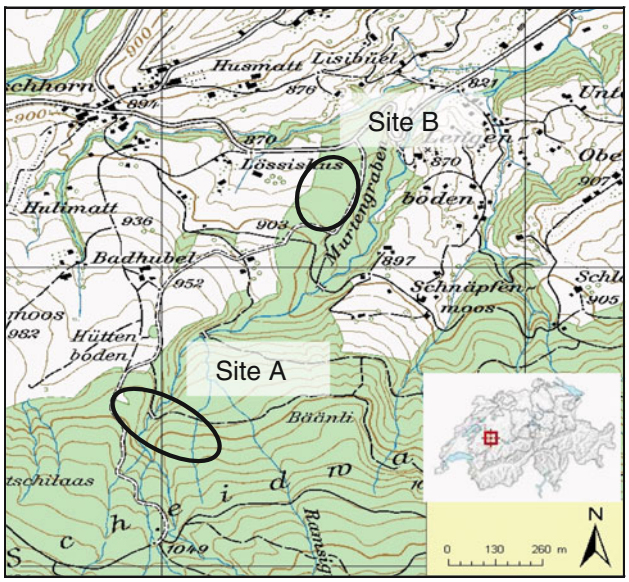

Fig. 1 Map of the investigated areas. Reproduced by permission of swisstopo (BA12053)

Table 1 Characteristics of the study sites

	Study site	
	A	B
Altitude (m) a.s.l.	≈1,000	≈880
Slope °	<15	<7
Soil types	Gleys, cambic Gleys, gleyic or stagnic Cambisols, Cambisols	Gleys
Forest community	Vaccinio myrtillii-Abieti-Piceetum	Luzulo-Abieti-Fagetum
Main tree species	Norway spruce, silver fir	Silver fir, European beech
Number of irrigated plots	16	10

Below, periodically water saturated horizons dominate. The soil textures at sites A and B were comparable, but varied considerably within the sites (Fig. 3). The bulk density was equal at both study sites in the top- and subsoils, while pH tended to be higher at site A (Fig. 4).

Sprinkling experiments

We conducted sprinkling experiments to measure variations in the volumetric water content $\theta(Z, t)$ as a function of time (t) at various depths (Z). At site A, the volumetric water content was measured with TDR equipment (time domain reflectometry). The wave guides consisted of two paired stainless steel rods, 0.15 m long, 30 mm apart and 5 mm in diameter. A 50-Ω coax cable connected the rods to an SDMX 50 coaxial multiplexer controlled by a CR10X micro-logger. A Campbell TDR100 device (Campbell Scientific, Logan, USA) generated the electrical pulses and received the signals. The transfer function of Roth et al. (1990) was applied to calculate the volumetric water content. At site B, soil moisture was recorded with FDR equipment (frequency domain reflectometry) from Decagon Device (Pullman, USA). We used 10HS soil moisture sensors (0.1 m long) and collected data with an Em50 data logger. Dielectric permittivity was converted to volumetric water content by applying the transfer function of Topp et al. (1980). Variations in water content were recorded at 60 s intervals at both sites. The wave guides were installed horizontally from a trench into each soil genetic horizon according to the soil profile descriptions. Thus, depth of water-content probes varied between the investigated plots. Each soil profile was equipped with five probes, where a soil was composed of less than five horizons, the thickest layer was equipped with two wave guides one below the other.

The sprinkler device consisted of an aluminium plate (1 m × 1 m) perforated with 100 holes in a

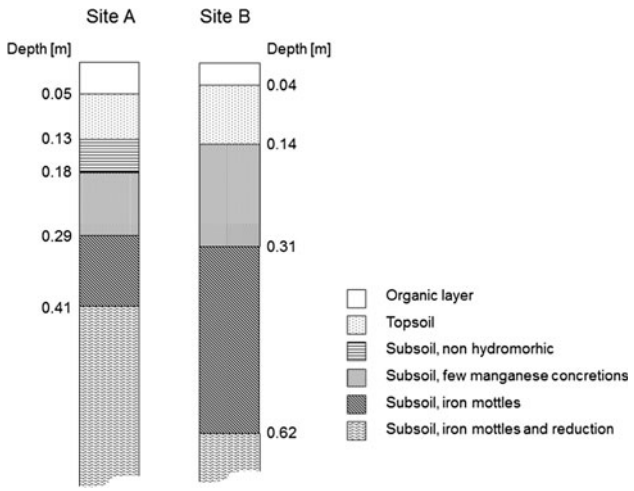

Fig. 2 Exemplary soil profiles and average depths of soil horizons at sites A and B

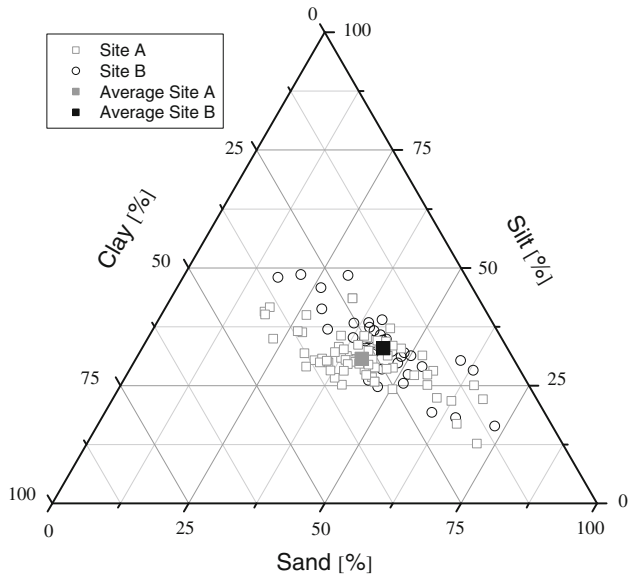

Fig. 3 Texture of all soil horizons at sites *A* and *B*

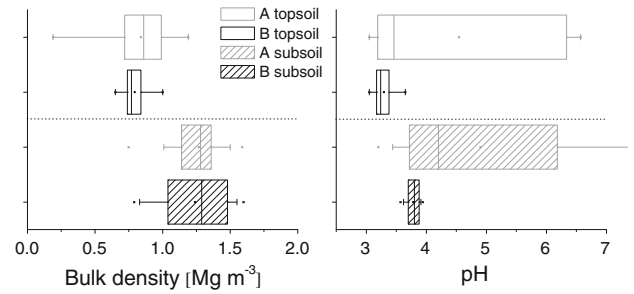

Fig. 4 Bulk density and pH ($CaCl_2$) at sites *A* and *B*, shown for topsoil and subsoil separately

0.1 m × 0.1 m square pattern. The holes were attached to PVC tubes (inner diameters 2 mm) connected to a water reservoir with a constant water table. The plate was moved by a motor ±50 mm back and forth in both horizontal dimensions during the irrigation experiments so that it took approximately 1,800 s until a tube returned to exactly the same position. The intensity of irrigation was 70 mm h^{-1} and lasted 1 h. No visible surface run-off occurred during the experiments. A waterproof tent (3 m × 3 m) covered the set-up and the soil profiles during the experiments.

At each plot, we conducted three consecutive irrigation experiments in 23 h intervals. The first and second irrigations primarily served to saturate the finer pores in the soil where capillarity may be dominant. As shown by Lange et al. (2011) at the same location, water flow released by the third artificial rainfall event was mainly restricted to larger, fast-draining pores, where capillarity can be neglected. Thus, the principal focus of our interpretation was on the results of the third irrigation, where the pore-size spectra of pores carrying mobile water were comparable in all plots and the influence of the varying antecedent soil moisture level was negligible.

Overall, we recorded 371 time series of water-content variations from 16 plots at site A and 10 plots at site B. The plots were distributed over an area of approximately 10,000 m^2 at site A and 2,000 m^2 at site B and the distances of the irrigated areas to the closest tree was about 1 m (with the exceptions of three plots at site A where the distance to the stem was about 3.5 m). The depths of the probes were between 0.04 and 0.97 m. We conducted the infiltration experiments in fall 2006 and summer and fall 2007 (site A), and in summer and fall 2010 (site B).

Root measurements

Soil cores for the analyses of the root length distribution were taken subsequent to irrigation with a HUMAX soil corer (diameter 0.1 m) to depths between 0.5 and 1 m, at the same positions as those where the TDR and FDR probes were installed. The cores consisted of 0.25 m long segments in plastic tubes in which the soil was left undisturbed. The roots were sorted out and washed in a 1-mm sieve with tap water. All root fragments (woody and herbal roots) were collected and stored at 4 °C for no more than 12 weeks. Root length (cm) was measured with win-RHIZO (V4.1c; Regent Instruments Inc., Quebec, Canada) for each morphological horizon separately.

Statistical analyses

To test distributions for different means, a rank-based test was applied (Mann–Whitney *U* test) since some data were not normally distributed. Statistical analyses were

conducted with SYSTAT (V10; Cranes Software International, Bangalore, India).

Theory

Infiltration was analysed according to a Stokes-flow approach. A steady water input during the period T_s [s], beginning at $t = 0$ [s], to the soil surface initiates a water-content wave (*wcw*, see Fig. 5a). The balance between gravity g as driving force and kinematic viscosity η, which expresses momentum dissipation, is what determines flow. Capillarity is neglected. The *wcw* consists of thin water films moving between two neighbouring layers (solid or gaseous phase). A water film is defined with its thickness f [m], its length of contact Λ [m] in the horizontal plane and the vertical position of the wetting front $z_w(t)$ [m] at time t (Fig. 6). A water film's specific contact length l [m^{-1}] is the contact area at time t between mobile water and the solid soil phase per soil volume, which corresponds to the length of contact Λ per horizontal two-dimensional extent of the soil A [m^2]:

$$l = \frac{\Lambda \cdot z_w(t)}{A \cdot z_w(t)} = \frac{\Lambda}{A} \quad (1)$$

where l describes porosity which effectively carries mobile water. Single water streaks are too tiny to be measured with ordinarily applied instrumentation such as TDR equipment. Superposition of all films adds up to the entire *wcw*, which is measurable in situ. An entire *wcw*'s contact length L [m^{-1}] per area A is:

$$L = \sum_A l \quad (2)$$

and its mobile water content per soil volume, which is the amplitude of infiltration ω_I [m^3 m^{-3}], is given by:

$$\omega_I = L \cdot F \quad (3)$$

where F is the water films' average thickness. According to Germann and al Hagrey (2008), the *wcw*'s average wetting front velocity from the soil surface to depth Z [m], v_W [m s^{-1}] is given by:

$$v_W = \frac{g}{3\eta} F^2 = \frac{Z}{t_W} \quad (4)$$

where g [9.81 m s^{-2}] is the acceleration due to gravity, η [10^{-6} m^2 s^{-1}] is the kinematic viscosity and t_W [s] is the arrival time of the wetting front. Rearranging Eq. (4) leads to F:

$$F = \left(3\frac{Z\eta}{t_W g}\right)^{0.5} \quad (5)$$

Contact length L can be determined by solving Eq. (3) for L:

$$L = \frac{\omega_I}{F} \quad (6)$$

See Germann et al. (2007) for further details. Stokes flow is amenable to a certain range in the soil water content between Darcy's saturated flow and a lower degree of saturation, where Richards' capillary equilibrium requirement remains valid. Thus, the approach used is limited to a soil moisture range where mainly larger, fast-draining pores are involved in water flow and capillary forces can be ignored. According to Hincapie and Germann (2009), a rainfall intensity of 5 mm h^{-1} may present the lower limit for producing significant water-content waves. The volume flux density of our irrigation experiments was 70 mm h^{-1}, and most likely resulted in *wcw*s amenable to Stokes flow.

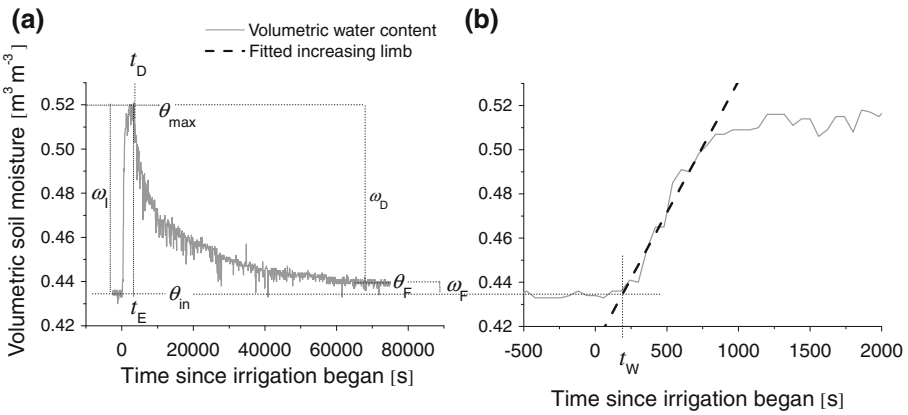

Fig. 5 **a** Definitions of parameters and variables of water-content waves (*wcw*). **b** Fitted increasing limb of a *wcw*. θ_{in} initial volumetric water content, θ_{max} maximum volumetric water content, θ_F volumetric water content 75,000 s after the irrigation began, ω_I $\theta_{max} - \theta_{in}$, amplitude of infiltration, ω_D $\theta_{max} - \theta_F$, amplitude of drainage, ω_F $\theta_F - \theta_{in}$, amount of non-draining water, t_w arrival time of wetting front, t_E end of irrigation at $t = 3{,}600$ s, t_D arrival time of the drainage front

Analyses of wcws

The key points of a *wcw*, initial (θ_{in}) and maximal (θ_{max}) water content were derived from the mean of ten water-content recordings between the beginning of the irrigation t_0 and $t_0 - 540$ [s] (θ_{in}) and between the arrival time of the drainage front t_D and $t_D - 540$ [s] (θ_{max}). The final water content θ_F refers to the interval between 74,460 and 75,000 s (see Fig. 5a), where water content was constant during data recording, θ_{max} was averaged over the last 540 s of the irrigation (3,060–3,600 s). A *wcw* is defined with its amplitudes of infiltration ω_I ($\theta_{max} - \theta_{in}$), which corresponds to the mobile water content (see Eqs. 3 and 6), and drainage ω_D ($\theta_{max} - \theta_F$) and the amount of non-draining water ω_F ($\theta_F - \theta_{in}$, Fig. 5a).

The calculations of film thickness F and contact length L require an increase in volumetric water content due to irrigation since F is given by the velocity of the wetting front and the calculation of L is based on F and the amplitude of infiltration (Eqs. 5 and 6). We defined a threshold value of $\omega_I = 0.01$ m^3 m^{-3} to separate non-reactive and reactive *wcw*s, and only *wcw*s with $\omega_I \geq 0.01$ m^3 m^{-3} were further analysed according to the Stokes-flow approach. In principle, t_W can be derived from *wcw*s with a maximum accuracy corresponding to the temporal resolution of the recordings. This may result in uncertainties if F is calculated according to Eq. (5) since the measurement intervals were 60 s. The approximately linear increasing limbs of the *wcw*s were therefore fitted by a linear function $\theta(t)$, and the point in time when $\theta(t) = \theta_{in}$ is the arrival time of the wetting front t_W:

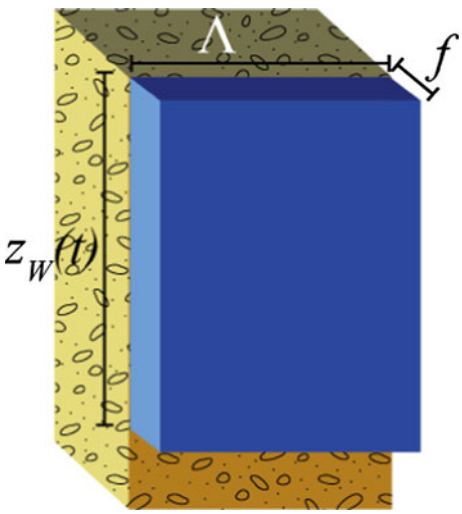

Fig. 6 Geometry of a water film flowing along a vertical plane. f film thickness, Λ length of contact between mobile water and the resting part of the soil in the horizontal plane; $z_W(t)$ vertical position of the wetting front as a function of time t

$$t_W = \frac{\theta_{in} - b}{a} \quad (7)$$

where a is the slope [dθ dt^{-1}] and b is the y intercept of the linear fitting function. Figure 5b) shows the fitted increasing limb of a *wcw* and the corresponding t_W.

Knowing t_W and depth Z, F follows from Eq. (5). Contact length L is determined according to Eq. (6), including F and the amplitude of infiltration ω_I, which corresponds to the mobile water content.

Since F and L are calculated according to the maximal velocity of the wetting front (Eq. 5) between the soil surface and depth Z and on measured volumetric water content at Z (Eq. 6), L and F are also controlled by the wetting front's advance and the water-carrying porosity above Z, which has to be considered when interpreting the water-flow geometry.

Results

Water-content waves

Table 2 lists the number of recorded *wcw*s and the arithmetic means of θ_{in}, ω_I, ω_D and ω_F for sites A and B (see Fig. 5a), including the whole data set of recorded *wcw*s independent of measurement depths. Initial water content was significantly lower at site B for all irrigations. The amplitudes of infiltration and drainage were lower at site A than at site B, but only ω_I of the second irrigation differed significantly between the sites. Increasing the initial soil moisture reduced ω_I. The most marked decline of ω_I was found between the first and the second irrigation at site A, and between the second and the third irrigation at site B. For the first, second and third irrigation, 26.8, 36.7 and 40.5 %, respectively (site A), and 26.0, 24.5 and 32.6 %, respectively (site B) of all recorded *wcw*s were non-responsive to the irrigation (meaning $\omega_I < 0.01$ m^3 m^{-3}). Thus, the proportion of non-responsive *wcw*s increased with increasing antecedent soil moisture.

The distribution of ω_I versus soil depth differed substantially between the two study areas (Fig. 7). At site A, ω_I was clearly reduced at higher soil depths, while the averaged amplitudes of infiltration were approximately constant down to 0.7 m at site B. Thus, the infiltration capacity at site A was mainly limited to the upper soil horizons, while site B had higher ω_I between 0.3 and 0.7 m depth, resulting in larger infiltration capacities in the entire soil.

The required boundary conditions for water flow according to Eqs. (1–6) are: (i) an increase in the water content due to irrigation and (ii) gravity-driven flow instead of capillarity-dominated flow. As ω_F indicates, the saturation of finer pores was pronounced during the first and

Table 2 Number of recorded *wcw*s and arithmetic means of the water-content waves' amplitudes

Irr.	Recorded *wcw*s		θ_{in}			ω_I			ω_D			ω_F		
	Number		$m^3\ m^{-3}$			$m^3\ m^{-3}$			$m^3\ m^{-3}$			$m^3\ m^{-3}$		
	A	B	Ø A	Ø B		Ø A	Ø B		Ø A	Ø B		Ø A	Ø B	
1	71	50	0.399	0.301	***	0.057	0.062	n.s.	0.025	0.040	n.s.	0.031	0.022	n.s.
						26.8 %	*26.0 %*							
2	79	49	0.432	0.331	***	0.035	0.060	*	0.030	0.041	n.s.	0.005	0.019	**
						36.7 %	*24.5 %*							
3	79	43	0.434	0.336	***	0.034	0.045	n.s.	0.029	0.038	n.s.	0.004	0.007	n.s.
						40.5 %	*32.6 %*							

Irr irrigation, *Ø* arithmetic mean, *A* site A, *B* site B, θ_{in} initial water content, ω_I amplitude of infiltration, ω_D amplitude of drainage, ω_F non-draining water

* $p < 0.05$; ** $p < 0.01$; *** $p < 0.0001$; *n.s.* not significant

In italics: percentage of wcws with $\omega_I < 0.01\ m^3\ m^{-3}$

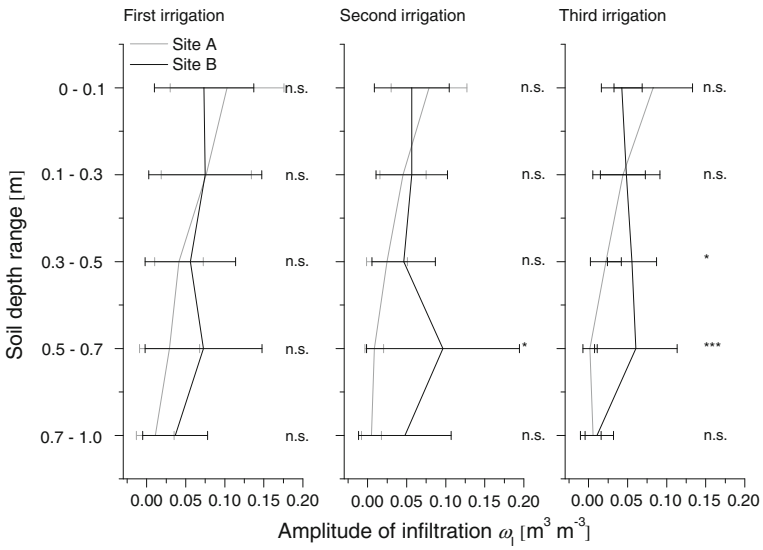

Fig. 7 Averaged amplitudes of infiltration ω_I at sites A and B for different soil depth ranges. n.s. not significant; *$p < 0.05$, ***$p < 0.001$

second irrigation at site B, but only during the first irrigation at site A. Thus, the calculation of *L* and *F* was limited to *wcw*s with $\omega_I \geq 0.01\ m^3\ m^{-3}$ for the third irrigation ($n = 47$ at site A and $n = 29$ at site B). Including all *wcw*s where film thicknesses and contact lengths were calculable, *F* and *L* did not significantly differ between the two sites (Mann–Whitney *U* test, $p \leq 0.05$). Nevertheless, the averaged film thicknesses at site B (1.90×10^{-5} m) exceeded those at site A (1.58×10^{-5} m) by approximately 20 %. *L* at site A exceeded those at site B by 18 % on average (4,804 m^{-1} at sites A and 4,081 m^{-1} at site B), but the median of *L* was larger at site B (3,030 m^{-1} at site A and 3,702 m^{-1} at site B). These differences in water-flow geometry resulted in higher amplitudes of infiltration at site B. The cumulative frequencies of *L*, *F* and ω_I are shown in Fig. 8.

L and *F* at depth *Z* are also controlled by the wetting front's advance above *Z*. Thus, only the relative progress of *L* and *F* versus soil depth was analysed. For this analysis, *F* and *L* were averaged for each depth range per site and divided by the arithmetic means of both sites' *F* and *L*. Figure 9 summarises the progress of *L* and *F* for five depth categories (0–0.1, 0.1–0.3, 0.3–0.5, 0.5–0.7 and 0.7–1.0 m depth). *F*, and thus the velocity of the wetting front (Eq. 4), was approximately constant over the entire soil depth at site A, except in topsoil horizons where film thicknesses were smaller. *F* at site B increased versus soil depth, and the water accelerated. *L* was less beneath 0.1 m at site A and at $Z > 0.5$ m at site B. The higher average *L* at site A was due to few extensive contact lengths in topsoils since *L* at site A was less at $Z > 0.1$ m compared with site B. In summary, the decreasing ω_I was due to the

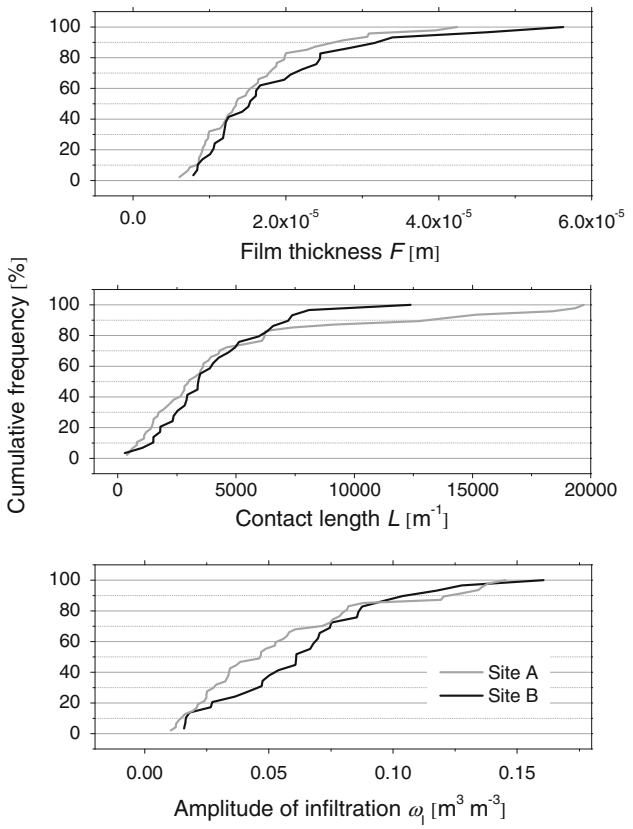

Fig. 8 Cumulative frequencies of contact lengths L, film thicknesses F and amplitudes of infiltration ω_I for the third irrigation at sites A ($n = 47$) and B ($n = 29$). Only water-content waves with $\omega_I \geq 0.01$ m^3 m^{-3} were considered

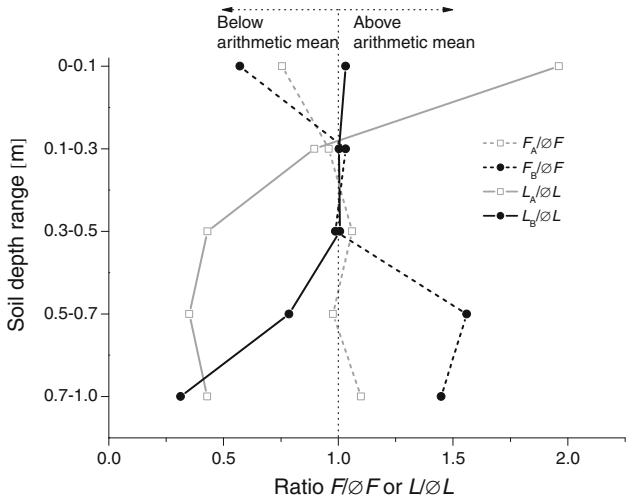

Fig. 9 Relative film thicknesses and contact lengths for sites A and B versus soil depth. F_A, F_B, L_A, L_B arithmetic means of the film thicknesses F and contact lengths L of the specific soil depth range at sites A (F_A, L_A) and B (F_B, L_B), $\varnothing F$ and $\varnothing L$ arithmetic means of the film thicknesses and contact lengths at the specific soil depth range, including both sites A and B

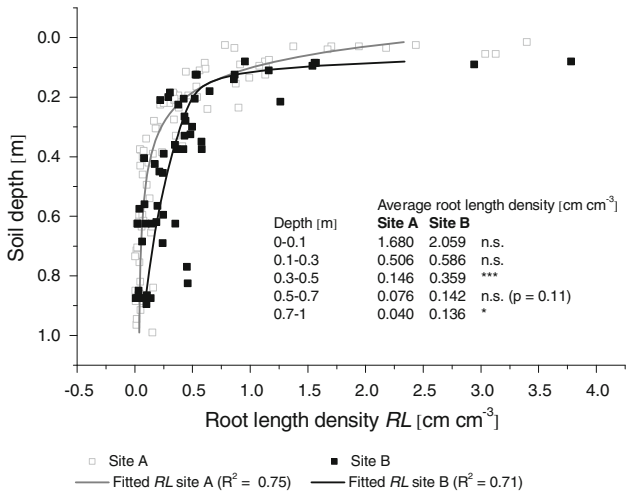

Fig. 10 Root length densities (RL) and fitted RL versus soil depth for sites A and B. n.s. not significant. *$p < 0.05$, ***$p < 0.001$

decreasing porosity carrying mobile water (L) at both sites, while film thicknesses were approximately constant (site A) or tended to increase with depth (site B).

Root densities

Including all soil depths, arithmetic means of root lengths per soil volume RL [cm cm^{-3}] did not differ distinctly between the two sites (averaged RL = 0.529 cm cm^{-3} for site A and 0.504 cm cm^{-3} for site B). However, RL versus soil depth varied markedly between the investigated forest stands. In comparison with site B, site A had larger root densities in topsoils but RL decreased more pronouncedly with increasing soil depth. Below 0.1 m depth, RL was on average smaller at site A (0.238 cm cm^{-3}) than at site B (0.332 cm cm^{-3}). At a depth range of 0.3–0.5 and 0.7–1.0 m, RL of site B was significantly higher than that of site A. Figure 10 summarises RL versus soil depth for sites A and B, including a fitting function of RL versus soil depth.

Soil properties influencing the amplitude of infiltration

We applied a multiple linear regression for the third irrigation to ascertain the parameters determining the amplitude of infiltration ω_I. The depth of the water-content probes, initial water content θ_{in}, root length density RL, bulk density BD and percentages of sand, silt and clay served as predictors. Some of the data were not normally distributed and square-root transformed to obtain approximately normal distributions (RL and depth at site A and RL at site B). Since some root data were not determinable at site A due to technical problems with the auger, the

universe at site A was 67 *wcw*s (out of 79) for the regression analyses, while all water-content recordings ($n = 43$) at site B were included. We applied a forward stepwise regression. Table 3 shows the resulting predictors and coefficients of determination for sites A and B. The first step of the regression led to the predictor which explains the maximum of ω_I's variance (RL at site A ($R^2 = 0.57$) and θ_{in} at site B ($R^2 = 0.09$)). Both relationships were significant at $p < 0.05$. The regression at site B could not be advanced by an additional predictor, whereas the regression coefficient at site A increased to $R^2 = 0.68$ by integrating silt content and to $R^2 = 0.75$ by including additional initial soil water content. More steps did not improve the regressions. Thus, root density mainly determined ω_I at site A, while such soil properties as texture, bulk density and root length density were not sufficient to describe the amplitude of infiltration at site B since only θ_{in} influenced ω_I significantly.

Predicted amplitude of infiltration with greater abundance of beech

Since root density was the main determiner of the amplitude of infiltration at the present coniferous stand (site A), it is feasible to model the expected ω_I at site A. RL versus soil depth was therefore fitted by second-order decay functions (Fig. 10), which are given by:

$$\mathrm{RL_A}(Z) = 0.0328 + 0.67514 \cdot \mathrm{e}^{\frac{-Z}{0.20057}} + 2.01966 \cdot \mathrm{e}^{\frac{-Z}{0.07938}} \quad (8)$$

and

$$\mathrm{RL_B}(Z) = -0.06243 + 39.49142 \cdot \mathrm{e}^{\frac{-Z}{0.02549}} + 0.79725 \cdot \mathrm{e}^{\frac{-Z}{0.54057}} \quad (9)$$

where Z is the soil depth [m] and A and B refer to sites A and B. The coefficient of determination R^2 was 0.75 for site A and 0.71 for site B. Based on the regression analyses shown in Table 3, the relationship between the present root density and the amplitude of infiltration at site A ($\omega_{I(pres)}$) is, considering square-root normalised data, given by:

Table 3 Multiple linear regression analyses with ω_I as the explanatory variable

Dependent variable ω_I	First step		Second step		Third step	
	Predictors	R^2	Predictors	R^2	Predictors	R^2
Site A	RL	0.57	RL, u	0.68	RL, u, θ_{in}	0.75
Site B	θ_{in}	0.09	–	–	–	–

ω_I Amplitude of infiltration, *RL* root length density, u percentage of silt, θ_{in} initial water content

$$\omega_{I(pres)}(Z) = 0.08463 \cdot (\mathrm{RL_A}(Z))^{\frac{1}{2}} - 0.00826 \quad (10)$$

We assume that the present root density at site A ($\mathrm{RL_A}$) will increase to that determined at site B ($\mathrm{RL_B}$) as beech becomes more abundant. Considering the predicted root density $\mathrm{RL_B}$ at site A, the predicted amplitude of infiltration $\omega_{I(pred)}(Z)$ is:

$$\omega_{I(pred)}(Z) = 0.08463 \cdot (\mathrm{RL_B}(Z)^{\frac{1}{2}} - 0.00826 \quad (11)$$

The averaged difference in ω_I between $\omega_{I(pres)}$ and $\omega_{I(pred)}$, $\omega_{I(dif)}$ from depths Z_1 to Z_2 is given by:

$$\omega_{I(dif)} = \frac{\int_{Z_1}^{Z_2} \omega_{I(pred)} - \omega_{I(pres)}}{Z_2 - Z_1} \quad (12)$$

and the additional water storage capacity due to the higher root density, $\mathrm{sc_{(add)}}$, between Z_1 and Z_2 is:

$$\mathrm{sc_{(add)}} = \omega_{I(dif)} \cdot (Z_2 - Z_1) \quad (13)$$

Figure 11 shows the fitted root densities according to Fig. 10, and the present and predicted amplitudes of infiltration based on Eqs. (10) and (11) for soil depths between 0.3 and 1.0 m. Site B clearly had significantly higher root densities (with the exception of the depth range of 0.5–0.7 m, where $p = 0.11$). It can be expected that ω_I would increase, on average, from the current 0.015–0.028 $\mathrm{m^3\ m^{-3}}$ at $0.3\ \mathrm{m} \le Z \le 1.0\ \mathrm{m}$, resulting in additional water storage capacity of 9.2 mm.

Figure 12 shows the predicted additional water storage capacity $\mathrm{sc_{(add)}}$ according to Eq. (13) for different soil depth ranges. Between 0.3 and 0.7 m depth, $\mathrm{sc_{(add)}}$ is relatively constant (1.48–1.68 mm per 0.1 m soil) and declines at $Z > 0.7$ m. Thus, an increase in infiltration capacity due to the greater abundance of beech is mainly restricted to soil depths between 0.3 and 0.7 m.

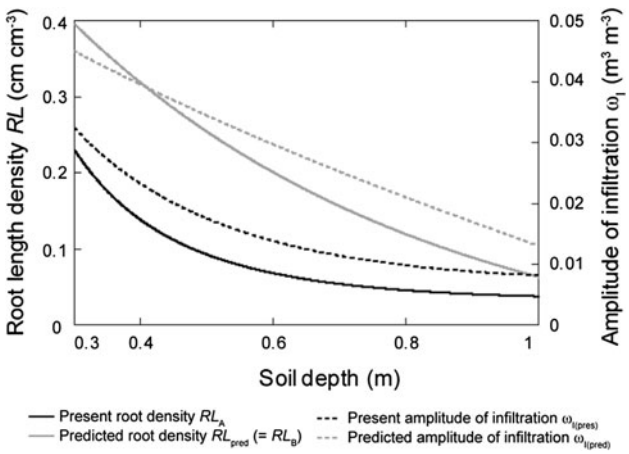

Fig. 11 Present ($\mathrm{RL_A}$) and predicted root density ($\mathrm{RL_{pred}} = \mathrm{RL_B}$) according to Eqs. (8) and (9), and present and predicted amplitudes of infiltration $\omega_{I(pres)}$ and $\omega_{I(pred)}$ according to Eqs. (10) and (11) for site A

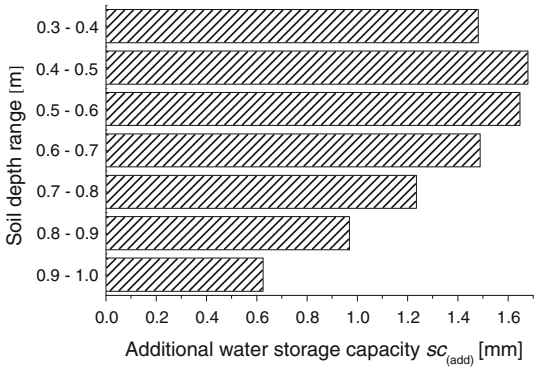

Fig. 12 Predicted additional water storage capacity $sc_{(add)}$ according to Eq. (13) for different soil depth ranges at site A

Discussion and conclusions

Infiltration properties

Averaged ω_I at the beech site (B) exceeded those at the spruce site (A) by 0.005, 0.025 and 0.011 $m^3\ m^{-3}$ for the first, second and third irrigation, respectively, due to the proportion of *wcw*s with no increase in water content being lower at site B and larger ω_I for water-content measurements with $\omega_I \geq 0.01\ m^3\ m^{-3}$. This was probably because the initial soil water contents were significantly lower at site B than at site A (about 0.1 $m^3\ m^{-3}$ for all irrigations). The total porosities of comparable hydromorphic soils measured in the Flysch zone were between 0.42 and 0.57 $m^3\ m^{-3}$ (Richard and Lüscher 1987). Thus, averaged θ_{in} at site B was presumably at least 0.08 $m^3\ m^{-3}$ below saturation since the mean of antecedent soil water content was at most 0.34 $m^3\ m^{-3}$, even for the third irrigation. Nevertheless, the volumes of non-draining water within approximately 20 h, ω_F, were close to zero for the third irrigation and did not differ significantly between sites A and B (Table 2). This observation suggests that mainly larger pores were involved in infiltration and the water-carrying pore-size spectra were comparable at both sites investigated for the third irrigation.

The bulk density and soil texture, and thus the total porosity, did not vary significantly between sites A and B. The fact that θ_{in} was lower for the third irrigation, although still with complete drainage, but ω_I was larger, indicates that there were proportionally more larger, fast-draining pores at site B than at site A. This interpretation is supported by the contact lengths since at site B, L was larger at a depth range of 0.1–0.7 m. Consequently, potential infiltration was mainly restricted to topsoils at site A, while ω_I was approximately constant down to a depth of 0.7 m at site B.

The interpretation of contact lengths and film thicknesses for the third irrigation gives additional information about water-flow geometry for *wcw*s with $\omega_I \geq 0.01\ m^3\ m^{-3}$ since the amplitude of infiltration is given by the product of L and F (Eq. 3). At site A, F, and accordingly the velocity of the wetting front (Eq. 4), was approximately constant between 0.1 and 1 m depth. Consequently, variations in ω_I were due to differing L, as Hincapie and Germann (2009) also found. At site B, film thicknesses increased between 0.5 and 0.7 m and, according to Eq. (4), wetting fronts accelerated, while L decreased. This was possibly due to water films flowing together when porosity was reduced in deeper soil, resulting in thicker films and increasing v_W (Eq. 4). This funnel effect requires well-connected pores. Since we did not detect such an acceleration of the wetting front at site A, we assume that the connectivity of vertical pores was less distinct at site A.

Root densities

Root densities were higher at site B, also in hydromorphic horizons. The forest sites investigated differed mainly in their abundances of beech and spruce since fir occurs in both forest communities. Accordingly, beech most likely had larger root densities, especially below depths of approximately 0.3 m. These findings are in accordance with those of Schmid and Kazda (2001), who observed that the relative number of spruce roots in mixed beech–spruce stands was lower than that of beech, and mainly concentrated in the upper soil. Furthermore, beech is less liable to temporarily anaerobic conditions in the rhizosphere than spruce (Lehnardt and Brechtel 1980). Soil acidity can substantially influence root growth and root distribution. Jentschke et al. (2001), for example, showed that fine root biomass in the mineral soil of Norway spruce forests was reduced in heavily acidified stands, but increased in organic layers. On the other hand, Finér et al. (2007) found no correlation between pH and root biomass in spruce and beech stands but demonstrated that root biomass in beech stands exceed that of spruce stands markedly. In this study, the root density was higher at the more acid site B. Consequently, the difference in root densities between the two investigated sites could have been even stronger if soil acidity would have been comparable. Thus, infiltration capacity at the current coniferous site could possibly increase more strongly than we suggested when beech will be more abundant due to climate change.

Soil properties influencing the amplitude of infiltration

At site A, the root length density was the most significant predictor of ω_I, as many other studies that focused on the influence of roots on soil water flow have also found (e.g. Angers and Caron 1998; Perillo et al. 1999). It is then most

likely that roots generated the porosity accessible to water. According to the Stokes-flow approach, the amplitude of infiltration ω_I is given by the product of L and F (Eq. 3). Thus, for *wcw*s with $\omega_I \geq 0.01$ m^3 m^{-3}, where L and F were calculable, the root densities may be related to film thickness, contact length or both parameters. Since L was clearly related to RL ($R^2 = 0.43$), but the coefficient of regression between F and RL was only 0.03, we draw the conclusion that the porosity carrying mobile water was indeed mainly generated by roots. Our investigations were conducted on a plot scale. This raises the question whether the impact of roots on soil hydrology can be assessed on larger scales in a similar way to the approach used in this study. The key issue is if the root densities measured at particular soil depths are the representative of the entire stand's root densities. According to Brunner et al. (2004), the number of fine root segments is independent of their distance from the nearest tree in a forest community very similar to site A. Fine roots accounted for approximately 90 % of total root length density at site A, where ω_I was determined by root densities. Thus, we can assume that the observed root densities based on 16 (site A) and 10 (site B) soil profiles represent the stand's root density well enough.

The predictors applied did not enable ω_I to be predicted well at site B. Larger pores, where water flow is gravity driven, can also be generated by physical processes such as thawing and freezing (Beven and Germann 1982) or shrinking and swelling (Romkens and Prasad 2006), or by biological factors such as earthworms (e.g. Lamande et al. 2003). Earthworms were not found during soil excavation at site B, possibly because of the soils low pH (Potthoff et al. 2008). Since bedrock, soil genesis, soil properties such as bulk density and texture, as well as climatic conditions, are similar at both sites, no significant differences in pore-generating processes besides roots are expected. The current root density does not necessarily represent total porosity generated by roots since decomposed roots are also able to generate pores accessible to water (Jorgensen et al. 2002). Thus, it may be possible that, even at site B, pores carrying mobile water were mainly generated by roots, but with the method of root measurement we used, decayed roots could not be detected.

Schwarzel et al. (2009) showed that the spatial distribution of soil–water variability in spruce and beech stands was related to not only soil properties but also to root distributions due to the water uptake of trees. The daily transpiration rates of beech stands can exceed 5 mm when water availability is sufficient (Marc and Robinson 2004), while spruce forests transpire at most 1.5–2 mm day^{-1} (Clausnitzer et al. 2011). Since the mobile water content was significantly influenced by the initial soil water content at site B and, to a lesser extent, also at site A, roots indirectly affect ω_I by modifying the antecedent soil moisture due to water uptake. Thus, beech will reduce θ_{in} during the growing season more than spruce and will make additional water storage capacity available, which will decrease during winter and early spring when beech hardly transpires.

In this study, we focused on the significance of different species' roots for gravity-driven water flow in soils, but the predicted transformation of forests can also affect the soil's hydrological properties via other processes. These processes include the varying characteristics of organic layers (Greiffenhagen 2005) and the trees' interception efficiency (Schume et al. 2003). The porosity generated by roots may also increase lateral water flow (Redding and Devito 2010) and therefore promote run-off generation (Uchida et al. 2005).

Change in water storage capacity

The greater abundance of beech in coniferous flood protection forests leads to increase in root densities and thus to an additional water storage capacity of 9–10 mm for soil depths between 0.3 and 1.0 m. Thus, the soil water storage capacity will be increased by approximately 15 % of a 1-h heavy precipitation with a recurrence interval of 100 years. Moreover, the initial water content will be reduced during the growing season because of the higher transpiration rates of beech, resulting in even more water storage capacity.

During forest transformation, beech and spruce will presumably coexist during a certain time period in the current coniferous stand. As shown by Schmid and Kazda (2002), fine root density in mixed beech–spruce forests growing on stagnic Cambisols was almost twice that of monospecific spruce stands. Thus, within a certain time period during forest transformation when beech initially grows in current coniferous forests, water storage capacity would possibly increase more than suggested by this study.

It is assumed, however, that climate change will lead to more frequent and intense heavy rainfall events (OcCC/ProClim-(ed.) 2007). Hence, even with greater infiltration capacity, the flood protection provided by a forest would not necessarily become more effective with the higher root densities associated with the predicted species shift, but the negative effects of more intense rainfall may be mitigated.

Hydrological models normally include vegetation by considering the transpiration rate which can be determined, for example, by root depth, leaf area index and potential evapotranspiration (e.g. Abbaspour et al. 2007). The results presented in this paper indicate that also modifications in porosity generated by roots substantially influence infiltration properties. Considering root distribution versus soil depth in water-flow models will not only enhance the assessment of transpiration rates but also the estimation of the significance of a modified pore system due to land use

change or forest transformation. Thus, more detailed information about root distribution in different forest stands may increase the validity of such models considerably.

This study has begun to investigate the impact of a forest transformation on infiltration due to the different root densities of the main tree species. To assess the significance of more abundant beech in coniferous flood protection forests, future investigations should be more comprehensive. They should, for example, include further factors that affect infiltration such as transpiration, interception and organic layer, as well as the impacts of species transformation on the lateral subsurface flow, which may result in more peak flow generation.

Acknowledgments We are grateful to Philipp Mösch and Dieter Müller for allowing us access to the sites. We thank Roger Köchli and Marco Walser for the help in the field and Silvia Dingwall for proofreading this manuscript. Two reviewers are acknowledged for their helpful and constructive comments which substantially improved the manuscript. This study was supported by the COST Action E38 (Woody Root Processes) and the research programme Forests and Climate Change (Swiss Federal Institute for Forest, Snow and Landscape Research WSL and the Federal Office for the Environment FOEN).

References

Abbaspour KC, Yang J, Maximov I, Siber R, Bogner K, Mieleitner J, Zobrist J, Srinivasan R (2007) Modelling hydrology and water quality in the pre-alpine/alpine Thur watershed using SWAT. J Hydrol 333:413–430

Angers AD, Caron J (1998) Plant-induced changes in soil structure: processes and feedbacks. Biogeochemistry 42(1–2):55–72

Bens O, Wahl NA, Fischer H, Huttl RF (2007) Water infiltration and hydraulic conductivity in sandy cambisols: impacts of forest transformation on soil hydrological properties. Eur J Forest Res 126(1):101–109

Beven K, Germann P (1982) Macropores and water-flow in soils. Water Resour Res 18(5):1311–1325

Brändli U-B (ed) (2010) Schweizerisches Landesforstinventar. Ergebnisse der dritten Erhebung 2004–2006. Eidgenössische Forschungsanstalt für Wald, Schnee und Landschaft WSL, Birmensdorf. Bundesamt für Umwelt, BAFU, Bern

Brunner I, Ruf M, Luscher P, Sperisen C (2004) Molecular markers reveal extensive intraspecific below-ground overlap of silver fir fine roots. Mol Ecol 13(11):3595–3600. doi:10.1111/j.1365-294X.2004.02328.x

Brzeziecki B, Kienast F, Wildi O (1995) Modeling potential impacts of climate-change on the spatial-distribution of zonal forest communities in Switzerland. J Veg Sci 6(2):257–268

Christiansen JR, Elberling B, Jansson PE (2006) Modelling water balance and nitrate leaching in temperate Norway spruce and beech forests located on the same soil type with the CoupModel. For Ecol Manage 237(1–3):545–556. doi:10.1016/j.foreco.2006.09.090

Clausnitzer F, Koestner B, Schwaerzel K, Bernhofer C (2011) Relationships between canopy transpiration, atmospheric conditions and soil water availability—analyses of long-term sap-flow measurements in an old Norway spruce forest at the Ore Mountains/Germany. Agric For Meteorol 151(8):1023–1034. doi:10.1016/j.agrformet.2011.04.007

Doerr SH, Shakesby RA, Walsh RPD (2000) Soil water repellency: its causes, characteristics and hydro-geomorphological significance. Earth Sci Rev 51(1–4):33–65

Ellenberg H, Klötzli F (1972) Waldgesellschaften und Waldstandorte der Schweiz. Schweizerische Anstalt für das Forstliche Versuchswesen, Birmensdorf

FAO-UNESCO (1988) Soil map of the world, vol 60, revised legend. Soil map of the world. Food and Agriculture Organization of the United Nations FAO, Rome

Finér L, Helmisaari HS, Lõhmus K, Majdi H, Brunner I, Børja I, Eldhuset T, Godbold D, Grebenc T, Konôpka B, Kraigher H, Möttönen MR, Ohashi M, Oleksyn J, Ostonen I, Uri V, Vanguelova E (2007) Variation in fine root biomass of three European tree species: Beech (*Fagus sylvatica* L.), Norway spruce (*Picea abies* L. Karst.), and Scots pine (*Pinus sylvestris* L.). Plant Biosyst 141(3):394–405

Germann PF, al Hagrey SA (2008) Gravity-driven and viscosity-dominated infiltration into a full-scale sand model. Vadose Zone J 7(4):1160–1169. doi:10.2136/vzj2007.0172

Germann P, Helbling A, Vadilonga T (2007) Rivulet approach to rates of preferential infiltration. Vadose Zone J 6(2):207–220. doi:10.2136/vzj2006.0115

Greiffenhagen A (2005) Einfluss der Humusauflage auf das Benetzungsverhalten und den Wasserhaushalt von Kiefernstandorten. Bodenökologie und Bodengenese Heft 37 37 0663571, vol 132 S. Technische Universität, Berlin

Guevara-Escobar A, Gonzalez-Sosa E, Ramos-Salinas M, Hernandez-Delgado GD (2007) Experimental analysis of drainage and water storage of litter layers. Hydrol Earth Syst Sci 11(5):1703–1716

Hagedorn F, Bundt M (2002) The age of preferential flow paths. Geoderma 108(1–2):119–132

Hincapie I, Germann PF (2009) Impact of initial and boundary conditions on preferential flow. J Contam Hydrol 104(1–4):67–73

Jentschke G, Drexhage M, Fritz HW, Fritz E, Schella B, Lee DH, Gruber F, Heimann J, Kuhr M, Schmidt J, Schmidt S, Zimmermann R, Godbold DL (2001) Does soil acidity reduce subsoil rooting in Norway spruce (*Picea abies*)? Plant Soil 237:91–108

Jorgensen PR, Hoffmann M, Kistrup JP, Bryde C, Bossi R, Villholth KG (2002) Preferential flow and pesticide transport in a clay-rich till: field, laboratory, and modeling analysis. Water Resour Res 38(11):28-1–28-11

Lamande M, Hallaire V, Curmi P, Peres G, Cluzeau D (2003) Changes of pore morphology, infiltration and earthworm community in a loamy soil under different agricultural managements. Catena 54(3):637–649. doi:10.1016/s0341-8162(03)00114-0

Lange B, Luescher P, Germann PF (2009) Significance of tree roots for preferential infiltration in stagnic soils. Hydrol Earth Syst Sci 13(10):1809–1821

Lange B, Germann P, Lüscher P (2010) Einfluss der Wurzeln auf das Wasserspeichervermögen hydromorpher Waldböden. Schweizerische Zeitschrift für Forstwesen 161:510–516

Lange B, Germann PF, Lüscher P (2011) Runoff-generating processes in hydromorphic soils on a plot scale: free gravity-driven versus pressure-controlled flow. Hydrol Process 25:873–885. doi:10.1002/hyp.7873

Lehnardt F, Brechtel H-M (1980) Durchwurzelungs- und Schöpftiefen von Waldbeständen verschiedener Baumarten und

Altersklassen bei unterschiedlichen Standortverhältnissen. Allgemeine Forst- und Jagdzeitung 151:120–127

Li YM, Ghodrati M (1994) Preferential transport of nitrate through soil columns containing root channels. Soil Sci Soc Am J 58(3):653–659

Lüscher P, Zürcher K (2003) Waldwirkung und Hochwasserschutz: Eine differenzierte Betrachtungsweise ist angesagt. Berichte aus der Bayerischen Landesanstalt für Wald und Forstwirtschaft 40:30–33

Marc V, Robinson M (2004) Application of the deuterium tracing method for the estimation of tree sap flow and stand transpiration of a beech forest (Fagus silvatica L.) in a mountainous Mediterranean region. J Hydrol 285(1–4):248–259. doi:10.1016/j.jhydrol.2003.09.001

Noguchi S, Tsuboyama Y, Sidle RC, Hosoda I (1999) Morphological characteristics of macropores and the distribution of preferential flow pathways in a forested slope segment. Soil Sci Soc Am J 63(5):1413–1423

OcCC/ProClim (ed) (2007) Klimaänderung und die Schweiz 2050. Erwartete Auswirkungen auf Umwelt, Gesellschaft und Wirtschaft, Bern

Peck A, Mayer H (1996) Einfluss von Bestandesparametern auf die Verdunstung von Wäldern. Forstwiss Centbl 115:1–9

Perillo CA, Gupta SC, Nater EA, Moncrief JF (1999) Prevalence and initiation of preferential flow paths in a sandy loam with argillic horizon. Geoderma 89:307–331

Potthoff M, Asche N, Stein B, Muhs A, Beese F (2008) Earthworm communities in temperate beech wood forest soils affected by liming. Eur J Soil Biol 44(2):247–254. doi:10.1016/j.ejsobi.2007.05.004

Redding T, Devito K (2010) Mechanisms and pathways of lateral flow on aspen-forested, Luvisolic soils, Western Boreal Plains, Alberta, Canada. Hydrol Process 24(21):2995–3010. doi:10.1002/hyp.7710

Richard F, Lüscher P (1987) Physikalische Eigenschaften von Böden der Schweiz, vol 4. Eidg. Anstalt für das forstliche Versuchswesen, Birmensdorf

Romkens MJM, Prasad SN (2006) Rain Infiltration into swelling/shrinking/cracking soils. Agric Water Manage 86(1–2):196–205. doi:10.1016/j.agwat.2006.07.012

Roth K, Schulin R, Fluhler H, Attinger W (1990) Calibration of time domain reflectometry for water-content measurement using a composite dielectric approach. Water Resour Res 26(10):2267–2273

Schmid I, Kazda M (2001) Vertical distribution and radial growth of coarse roots in pure and mixed stands of *Fagus sylvatica* and *Picea abies*. Canadian J For Res-Revue Canadienne De Recherche Forestiere 31(3):539–548

Schmid I, Kazda M (2002) Root distribution of Norway spruce in monospecific and mixed stands on different soils. For Ecol Manage 159:37–47

Schume H, Jost G, Katzensteiner K (2003) Spatio-temporal analysis of the soil water content in a mixed Norway spruce (*Picea abies* (L.) Karst.)—European beech (*Fagus sylvatica* L.) stand. Geoderma 112(3–4):273–287

Schwärzel K, Menzer A, Clausnitzer F, Spank U, Häntzschel J, Grünwald T, Köstner B, Bernhofer C, Feger K-H (2009) Soil water content measurements deliver reliable estimates of water fluxes: a comparative study in a beech and a spruce stand in the Tharandt forest (Saxony, Germany). Agric For Meteorol 149(11):1994–2006. doi:10.1016/j.agrformet.2009.07.006

Topp GC, Davis JL, Annan AP (1980) Electromagnetic determination of soil-water content—measurements in coaxial transmission-lines. Water Resour Res 16(3):574–582

Uchida T, Meerveld IT, McDonnell JJ (2005) The role of lateral pipe flow in hillslope runoff response: an intercomparison of non-linear hillslope response. J Hydrol 311(1–4):117–133. doi:10.1016/j.jhydrol.2005.01.012

Zimmermann S, Luster J, Blaser P, Walthert L, Lüscher P (2006) Waldböden der Schweiz. Band 3. Regionen Mittelland und Voralpen. Waldböden der Schweiz Band 3 3 4743328, vol 847 S. Hep Verlag, Bern